Studies of an Extremely High Molar Extinction Coefficient Ruthenium Sensitizer in Dye-Sensitized Solar Cells

Xueju Lv,*,† Feifei Wang,‡ and Yunhui Li†,*

College of Chemistry, Jilin University, Changchun 130021, China, and School of Chemistry and Environmental Engineering, Changchun University of Science and Technology, Changchun 130022, China

ABSTRACT An extremely high molar extinction coefficient heteroleptic polypyridyl ruthenium sensitizer, featuring a conjugated electron-rich furan unit in its ancillary ligand, has been synthesized and demonstrated as an efficient sensitizer in dye solar cells. With a preliminary testing, we have reached 8.8 % overall power conversion efficiency measured in the air mass 1.5 global conditions. Transient photoelectrical decays and electrical impedance spectra were analyzed to picture the intrinsic physics of temperature-dependent photovoltage and photocurrent. A higher temperature will result in more electronic states in deep level and a faster charge recombination at the titania/dye/electrolyte interface at a given V_{oc}.

KEYWORDS: ruthenium sensitizer • furan unit • solar cell • high molar extinction coefficient • conversion efficiency • temperature-dependent

1. INTRODUCTION

Solar energy is one of the most promising future energy resources. Dye-sensitized solar cells (DSC) based on mesoporous nanocrystalline TiO_2 films have attracted intensive interest for scientific and industrial applications because of their high photoelectricity conversion efficiency and low production cost (1–3). Further development of this particular device toward more favorable character becomes a solid target for all the scientists in this field (4). It is noted that the DSC technology only reached respectable high efficiencies up to 11 % measured under the standard air mass 1.5 global (AM 1.5G) conditions, although this efficiency is still less than half the efficiency of the best traditional silicon solar cells, which can efficiently use the photons of sunlight up to 1 200 nm for electricity generation. In contrast to silicon solar cells, most of dye sensitizers in DSC lack the light-harvesting ability in the near-infrared region. Thus, enhancing the optical absorptivity of a stained mesoporous film seems to be a feasible strategy by employing high molar extinction coefficient sensitizers. It was explored that the light-harvesting capacity can be enhanced by further extending the conjugation length of the ancillary ligand (L), in Ru(dcbpy)(L)(NCS)$_2$ (where dcbpy is 4,4′-dicarboxylic acid-2,2′-bipyridine) photosensitizers. Recently, Wang reported a new dye C106 with a sulfur atom inserted between hexyl and thiophene (5). The measured molar extinction coefficient at 550 nm for C106 is 18.7×10^3 M^{-1} cm^{-1}.
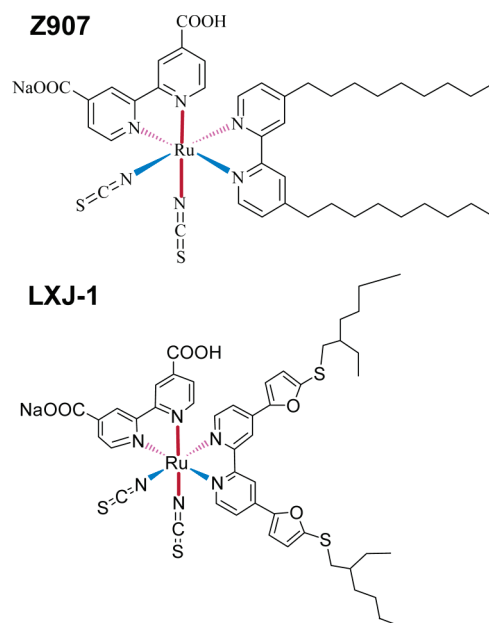

FIGURE 1. Molecular structures of Z907 and LXJ-1.

Here we report a novel heteroleptic ruthemium complex **LXJ-1** and shown in Figure 1. This new sensitizer features the electron-rich sulfur-furan unit conjugated with 2,2′-bipyridine, in contrast to the standard hydrophobic dye **Z907** with nonyl attached. Transient photoelectrical decay measurements and electrical impedance analysis have been performed to scrutinize the effects of the increasing temperature on the photovoltage and photocurrent.

2. EXPERIMENTAL SECTION

2.1. Materials. All solvents and reagents, unless otherwise stated, were of puriss quality and were used as received. N-Butyllithium and [RuCl$_2$ (p-cymene)]$_2$ were purchased from Aldrich. Sephadex LH-20 was obtained from Pharmacia. Guani-

dinium thiocyanate (GNCS), 3α,7α-dihyroxy-5β-cholic acid (cheno), and tert-butylpyridine (TBP) were purchased from Fluka. 1-Ethyl-3-methylimidazolium tetracyanoborate (EMITCB) and 400-nm-sized TiO_2 light-scattering paste were received as gifts from Dyesol. 1,3-Dimethylimidazolium iodide (DMII) and 1-ethyl-3-methylimidazolium iodide (EMII) were synthesized according to the literature method (6). 4,4′-Dibromo-2,2′-bipyridine, and N-butylbenzimidazole (NBB) were prepared according to the literature methods (7, 8).

2.2. Synthesis of 2-(Octan-3-ylthio) Furan. To a stirred solution of furan (10.83 g, 160 mmol) in anhydrous THF (150 mL) was added dropwise n-butyllithium (100 mL, 1.6 M in hexane, 1.0 equiv) at 0 °C under Ar. The mixture was warmed to room temperature and stirred for 2 h. After recooling the reaction mixtute to 0 °C, sulfur powder (6.74 g, 1.34 equiv) was added. The mixture was warmed to 0 °C and stirred for another 2 h. At last, 2-ethylhexyl bromide (27.92 mL, 1.0 equiv) was added portionwise at 0 °C and the mixture was stirred overnight at room temperature. The reaction was terminated by adding water. The mixture was extracted with CH_2Cl_2 and the combined organic layers were washed with water and dried over anhydrous Na_2SO_4. After rotary evaporation of solvents, the crude product was purified with column chromatography (petroleum ether) on silica gel to afford a yellowish liquid (23.6 g, 74.8 % yield). ^{1}H NMR (400 MHz, $CDCl_3$, δ_H): 7.47 (d, 1H), 6.44 (d 1H), 6.36(q, 1H), 2.77 (d, 1H), 1.42 (m, 4H), 1.25 (m, 6H), 0.88 (t, 3H), 0.84 (t, 3H). MS (ESI) m/z calcd for ($C_{12}H_{20}SO$): 212, Found: 213[M+ H]$^+$.

2.3. Synthesis of 4,4′-Bis(5-(octan-3-ylthio)furan-2-yl)-2,2′-bipyridine. N-Butyllithium (7.70 mL, 1.6 M in hexane, 12.24 mmol) was added dropwise to a solution of 2-(octan-3-ylthio) furan (2.00 g, 9.42 mmol) in anhydrous THF at −78 °C under Ar. The mixture was stirred at −78 °C for 1 h. After that, tributylstannyl chloride was added (3.57 mL, 13.18 mmol) and the mixture was stirred for 6 h at room temperature. The reaction was terminated by adding water. The mixture was extracted with ether and dried over anhydrous Na_2SO_4. After rotary evaporation of solvents, the crude tributyl (5-(octan-3-ylthio) furan-2-yl) stannane was mixed with 4,4′-dibromo-2,2′-bipyridine (0.98 g, 3.12 mmol), and $Pd(PPh_3)_2Cl_2$ (0.12 g, 0.17 mmol) in toluene (100 mL), and the mixture was refluxed under Ar overnight. After rotary evaporation of toluene under a reduced pressure, the resulting solid was purified by column chromatography on silica gel with methanol/chloroform (1/10) as eluent to afford the title compound (1.69 g, 94.4 % yield). ^{1}H NMR (400 MHz, $CDCl_3$, δ_H): 8.70 (d, 2H), 8.62 (s, 2H), 7.57 (q, 2H), 7.00 (d, 2H), 6.56 (d, 2H), 2.91 (d, 2H), 1.58 (m, 4H), 1.46 (m, 8H), 1.28 (m, 8H), 0.89 (t, 12H). MS (ESI) m/z calcd. for ($C_{34}H_{44}N_2O_2S_2$): 578, Found: 579 [M+ H]$^+$.

2.4. Synthesis of NaRu(4,4′-Bis(5-(octan-3-ylthio)furan-2-yl)-2,2′-bipyridine)(4-carboxylic acid-4′-carboxylate-2,2′-bipyridine)(NCS)$_2$ (LXJ-1). Dichloro(p-cymene)ruthenium(II) dimer (0.106 g, 0.17 mmol) and 4,4′-bis(5-(octan-3-ylthio)furan-2-yl)-2,2′-bipyridine (0.200 g, 0.34 mmol) were dissolved in DMF (40 mL). The reaction mixture was stirred at 60 °C for 4 h under Ar in the dark. Subsequently, 4,4′-dicarboxylic acid-2,2′-bipyridine (0.085 g, 0.34 mmol) was added into the flask and the reaction mixture was stirred at 140 °C for 4 h. At last, an excess of NH_4NCS (1.056 g, 13.87 mmol) was added to the resulting dark solution and the reaction was continued for another 4 h at the same temperature. Then, the reaction mixture was cooled to room temperature and the solvent was removed on a rotary evaporator. Water was added to obtain a suspended solution. The solid was collected on a sintered glass crucible by suction filtration, washed with water and ether, and dried under a vacuum. The crude complex was dissolved in basic methanol (NaOH) and purified on a Sephadex LH-20 column with methanol as eluent. The collected main band was concentrated and slowly titrated with an acidic water solution (HNO_3) to pH 4.2.

The precipitate was collected on a sintered glass crucible by suction filtration and dried in air. Yield with three times column purification: 40.4 %. ^{1}H NMR (400 MHz, CD_3OD + NaOH δ_H): 9.69.(d, 1H), 9.22 (d, 1H), 9.07 (s, 1H), 8.89(s, 1H), 8.39 (d, 1H), 8.36 (d, 1H), 8.20 (s, 1H), 7.77 (s, 1H), 7.63 (m, 4H), 7.29(d, 1H), 7.03 (s, 1H), 6.94(d, 1H), 6.84 (s, 1H), 3.23 (s, 1H), 3.10 (t, 1H), 1.59 (m, 8H), 1.44 (s, 4H), 1.33 (s, 4H), 1.06(t, 4H), 0.94(m, 12H). Anal. Calcd. For: $NaRuC_{48}H_{51}N_6O_6S_4 \cdot 2H_2O$: C, 52.59; H, 5.06; N, 7.67 %. Found: C, 52.50; H, 5.12; N, 7.60 %. MS (ESI) m/z calcd. for ($NaRuC_{48}H_{51}N_6O_6S_4$): 1060, Found: 1237 [M-Na]$^-$.

2.5. UV−Vis and Voltammetric Measurements. Electronic absorption spectra were recorded on a UNICO WFZ UV-2802PC/PCS spectrometer. A computer-controlled CHI660C electrochemical workstation was employed for square-wave voltammetric measurements with a three-electrode electrochemical cell.

2.6. Device Fabrication. A screen-printed single or double layer film of interconnected TiO_2 particles was used as mesoporous negative electrode. A 10 μm thick film of 20-nm-sized TiO_2 particles were first printed on the fluorine-doped SnO_2 (FTO) conducting glass electrode and further coated by a 5 -μm thick second layer of 400 nm sized light scattering anatase particles if it is needed. The film thickness was measured by a benchtop Ambios XP-1 stylus profilometer. The detailed preparation procedures of TiO_2 nanocrystals, pastes for screen-printing, and nanostructured TiO_2 film have been reported in the literature procedure (9). A cycloidal TiO_2 electrode (~0.28 cm^2) was stained by immersing it into a dye solution containing **Z907** or **LXJ-1** sensitizer (300 μM), cheno (2 mM) and TBAOH (150 μM) in a mixture of acetonitrile and tert-butanol (volume ratio: 1/1) overnight. After washing with acetonitrile and drying by air flow, the sensitized titania electrode was assembled with a thermally platinized FTO electrode. The electrodes were separated by a 30 μm thick Bynel (DuPont) hot-melt gasket and sealed up by heating. The internal space was filled with a liquid electrolyte using a vacuum backfilling system. The electrolyte-injecting hole on the counter electrode glass substrate, made with a sand-blasting drill, was sealed with a Bynel sheet and a thin glass cover by heating. Two electrolytes were used for device evaluations. Electrolyte A: 1.0 M DMII, 50 mM LiI, 30 mM I_2, 0.5 M tert-butylpyridine and 0.1 M GNCS in the mixed solvent of acetonitrile and valeronitrile (v/v, 85/15). Electrolyte B: DMII/EMII/EMITCB/I_2/NBB/GNCS (molar ratio: 12/12/16/1.67/3.33/0.67). Devices A and B were made with electrolyte A, employing the **LXJ-1** and **Z907** sensitizers, respectively. Device C was made with the **LXJ-1** sensitizer in combination with electrolyte B.

2.7. Photovoltaic Characterization. A LS100 solar simulator (Solar Light Com. Inc., USA) was used to give an irradiance of 100 mW cm^{-2} (the equivalent of one sun at AM1.5G) at the surface of a testing cell. The current−voltage characteristics were obtained by applying external potential bias to the cell and measuring the dark current and photocurrent with a Keithley model 2602 digital source meter. This process was fully automated using Labview 8.0. A similar data acquisition system was used to control the incident photon-to-collected electron conversion efficiency (IPCE) measurement. Under full computer control, light from a 1000 W xenon lamp was focused through a monochromator onto the photovoltaic cell under test. A computer-controlled monochromator (Omni λ300) was incremented through the spectral range (300−900 nm) to generate a photocurrent action spectra with a sampling interval of 10 nm and a current sampling time of 2 s. IPCE is defined by IPCE(λ) $= hcJ_{sc}/e\phi\lambda$, where h is the Planck constant, c is the light speed in vacuum, e is the electronic charge, λ is the wavelength (m), J_{sc} is the short-circuit photocurrent density (A m^{-2}), and ϕ is the incident radiative flux (W m^{-2}). Photovoltaic performance was measured by using a metal mask with an aperture area of 0.158

cm². A homemade heating−cooling system was used for temperature-dependent $J−V$ measurements.

2.8. Transient Photoelectrical Measurements. In transient photoelectrical decay experiments, a steady light was supplied with a white light-emitting diode (LED) array while a perturbing light pulse was provided with a green LED array controlled by a fast solid-state switch. Both white and green lights were irradiated on the photoanode side of a testing cell. The green pulse was carefully controlled by the driving potential of diodes to keep the modulated photovoltage below 5 mV. We used green light as a probe to generate a photovoltage perturbation near the open-circuit photovoltage (V_{oc}) of the cell under the white light and measured the voltage decay process thereafter. Normally, the transient signals follow a monoexponential decay, thus the recombination rate constant (k_r) can be extracted from the slope of the semilogarithmic plot. The capacitance (C_μ) of the titania interface at the V_{oc} are calculated by $C_\mu = \Delta Q/\Delta V$, where ΔV is the peak of the photovoltage transient and ΔQ is the number of electron injected during the green light flash. The latter is obtained by integrating a short-circuit photocurrent transient generated from an identical green pulse. This method may underestimate the actual injected electrons by the fraction that is lost due to recombination during the electron collection. The error is thought to be less than 30 % in the worst case. More critically, it does not affect the shape of the calculated capacitance versus potential but only the magnitude. A homemade heating−cooling system was used for temperature-dependent measurements.

2.9. Electrical Impedance Measurements. Electrical impedance experiments were carried out in the dark with an IM6ex electrochemical workstation, with a frequency range from 50 mHz to 100 kHz and a potential modulation of 10 mV. The obtained impedance spectra were fitted with the Z-view software (v2.80, Scribner Associates Inc.) in terms of appropriate equivalent circuits. A homemade heating−cooling system was used for temperature-dependent measurements.

3. RESULTS AND DISCUSSION

To gain insight into light-harvesting capacity of dye **LXJ-1**, we first measured the electronic absorption spectrum of the dye dissolved in DMF. As shown in Figure 2A, the intense absorption bands at 309 and 353 nm in the UV region are due to intraligand ($\pi \rightarrow \pi^*$) charge transitions of the dcbpy and conjugated ancillary ligands and furthermore, there are characteristic metal-to-ligand charge-transfer transition (MLCT) bands in the visible region like other heteroleptic polypyridyl ruthenium(Π) complexes (10). In DMF, the low energy MLCT transition absorption of **LXJ-1** peaks at 549 nm, which is 28 nm red-shifted compared to **Z907**. The measured peak molar extinction coefficient (ε) for **LXJ-1** is 18.4×10^3 M⁻¹ cm⁻¹, which is obviously higher than the corresponding values for **Z907** (12.2×10^3 M⁻¹ cm⁻¹ at the peak of 521 nm).

It is known that besides the molar extinction coefficient, the molecular size and packing mode also have a strong influence on the optical absorptivity of a stained mesoporous film. So we further investigated the film absorption which is more closely related to the light-harvesting of dye-sensitized solar cells. The film is sensitized by immersing it into a dye solution containing **Z907** or **LXJ-1** sensitizer (300 μM) in a mixture of acetonitrile and *tert*-butanol (volume ratio: 1/1) overnight. The striking improvement of introducing sulfur-furan via extending the π-conjugated system of ancillary ligands in heteroleptic ruthenium complexes can
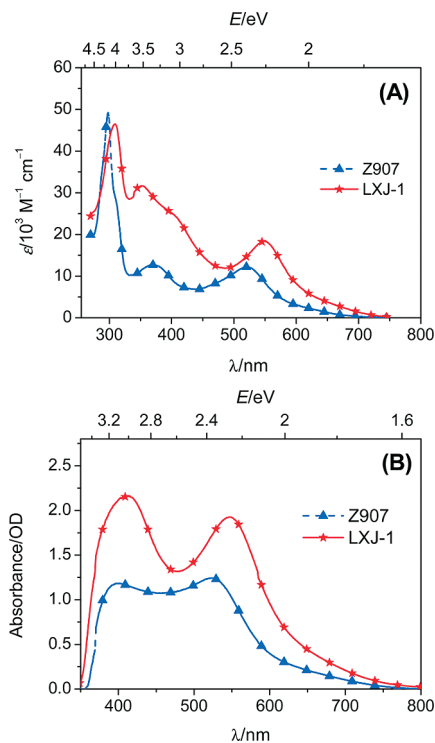

FIGURE 2. (A) Electronic absorption spectra of Z907 and LXJ-1 dissolved in DMF. (B) Absorption spectra of Z907 and LXJ-1 anchored on a 7.5 μm thick mesoporous titania film.
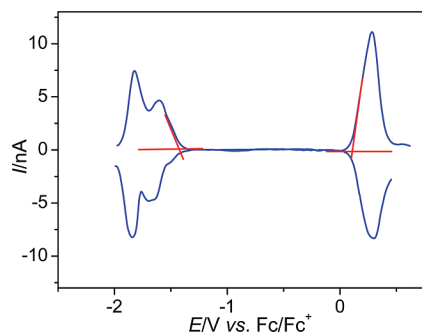

FIGURE 3. Square-wave voltammogram of a Pt ultramicroelectrode in a DMF solution containing the LXJ-1 dye and 0.1 M n-tetrabutyl-ammonium hexafluorophosphate as supporting electrolyte. The LUMO and HOMO were estimated vs vacuum: $E_{LUMO/HOMO} = -4.88 - F\phi_{redox}$.

be unambiguously perceived from Figure 2B, which depicts the absorption spectra in the visible region of **Z907** and **LXJ-1** anchored on a 7.5 μm thick transparent nanocrystalline TiO₂ film. Notably, the red-shifted and enhanced absorption peaks are observed, indicating a good charge collection yield for a high efficiency DSC. The film absorbance ratio of low-energy peaks for **Z907** and **LXJ-1** sensitizers is 1:1.55.

We employed square-wave voltammetry in combination with the ultramicroelectrode technique to measure the redox potentials of the **LXJ-1** sensitizer in a glovebox full of nitrogen. As depicted in Figure 3, the negative offset by the measured LUMO (-3.45 eV vs vacuum) of the **LXJ-1** dye with respect to the conduction band edge (-4.00 eV vs vacuum) (11) of titania supplies a thermodynamic driving force for charge generation. The thermodynamic and kinetic analyses suggest a possibility of ultrafast interfacial electron
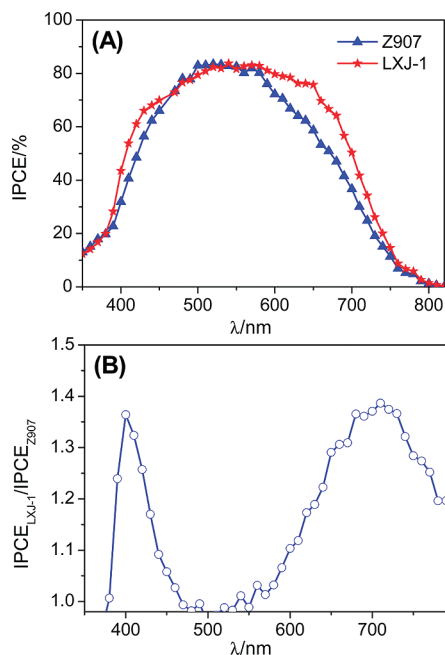
FIGURE 4. (A) Photocurrent action spectra of devices A and B made from LXJ-1 and Z907. (B) Relative monochromatic incident photon-to-collected electron conversion efficiencies.
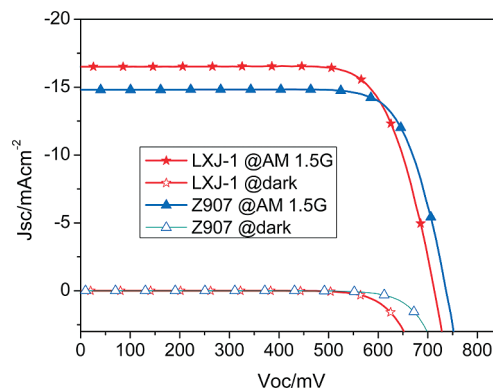

FIGURE 5. $J-V$ characteristic of devices A and B with LXJ-1 and Z907 measured under an irradiance of 100 mW cm^{-2} AM 1.5G sunlight. The aperture area of the testing mask: 0.158 cm^2. Film thickness: 10 + 5. An antireflection film was adhered to the cell during measurements. The electrolyte A composition is as follows: 1.0 M DMII, 50 mM LiI, 30 mM I$_2$, 0.5 M *tert*-butylpyridine, and 0.1 M GNCS in the mixed solvent of acetonitrile and valeronitrile (*v/v*, 85/15).

Table 1. Photovoltaic Performances of Devices A and B Based on LXJ-1 and Z907 Dyes under AM 1.5G Illumination (100mW cm^{-2})

sensitizer	V_{oc} (mV)	J_{sc} (mA cm^{-2})	FF	η (%)
LXJ-1	715.82	16.50	0.745	8.80
Z907	736.6	14.80	0.770	8.39

Z907 are 14.8 mA cm^{-2}, 736.6 mV, 0.770, and 8.39%, respectively. It is observed that the short-circuit photocurrent becomes high while the open-circuit photovoltage becomes low along with extending the π-conjugation and geometric enlargement of sensitizers. Overall, the enhanced J_{sc} may be due to better light harvesting.

We further measured the $J-V$ characteristics (Figure 6) at different temperatures for the device A with the **LXJ-1** dye. Obviously, the efficiencies of DSC exhibit remarkable stability with a fluctuation of temperature. Error bar of efficiencies of the device A at various temperatures is shown in Figure 7. The overall power conversion efficiencies at temperatures from −20 to 50 °C are over 8.0%, with a maximum of 8.96% at 0 and 10 °C. Relatively lower efficiency at 60 °C
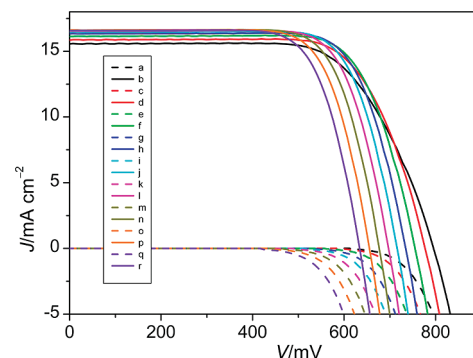
injection from the exited dye to the titania conduction band, before the occurrence of other radiative or nonradiative deactivation of excitons. The positive offset by the HOMO of **LXJ-1** (−5.00 eV vs vacuum) in contrast to that (−4.65 eV) of iodide (12) could lead to fast dye regeneration, avoiding the geminate charge recombination between oxidized dye molecules and photoinjected electrons in the nanocrystalline titania film.

To see the effect of light-harvesting enhancement from the π-conjugation extension, photocurrent action spectra of devices A and B, employing an acetonitrile-based electrolyte, along with the corresponding **LXJ-1** and **Z907** sensitizers were first measured as shown in Figure 4A. The monochromatic incident photon-to-collected electron conversion efficiencies of **LXJ-1** have exceeded 75% from 480 to 650 nm and exhibited a maximum efficiency of 83.7%. Considering the light absorption and scattering loss by the conducting glass, the absorbed photon-to-collected electron conversion efficiencies (APCE) are close to unity over a broad spectral range, suggesting a very high charge collection yield. A close look on the IPCE ratios (Figure 4B) of **LXJ-1** to **Z907** has explicitly demonstrated the remarkable merit of extending the π-conjugation of ancillary liagands in polypyridyl ruthenium sensitizers, especially in the red region of weak absorption and the blue region where competitive triiodide absorption is dissipative.

The $J-V$ characteristics of devices A and B are shown in Figure 5, and the detailed parameters are listed in Table 1. Under standard global AM 1.5G solar conditions, the short-circuit photocurrent density (J_{sc}), open-circuit photovoltage (V_{oc}) and fill factor (FF) of a cell made from **LXJ-1** are 16.50 mA cm^{-2}, 715.8 mV and 0.745 respectively, which yields an overall conversion efficiency (η) of 8.8%. In contrast, the photovoltaic parameters (J_{sc}, V_{oc}, FF, and η) of a cell with

FIGURE 6. $J-V$ characteristics of device A based on the LXJ-1 dye measured in the dark (dash curves a, c, e, g, i, k, m, o, and q) and under an irradiance of 100 mW cm^{-2} AM 1.5G sunlight (solid curves b, d, f, h, j, l, n, p, and r) at various temperatures: (a, b) 253 K; (c, d) 263 K; (e, f) 273 K; (g, h) 283 K; (i, j) 293 K; (k, l) 303 K; (m, n) 313 K; (o, p) 323 K; (q, r) 333 K. The electrolyte A composition is as follows: 1.0 M DMII, 50 mM LiI, 30 mM I$_2$, 0.5 M *tert*-butylpyridine, and 0.1 M GNCS in the mixed solvent of acetonitrile and valeronitrile (*v/v*, 85/15).
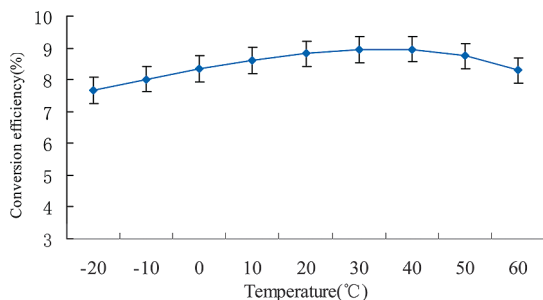
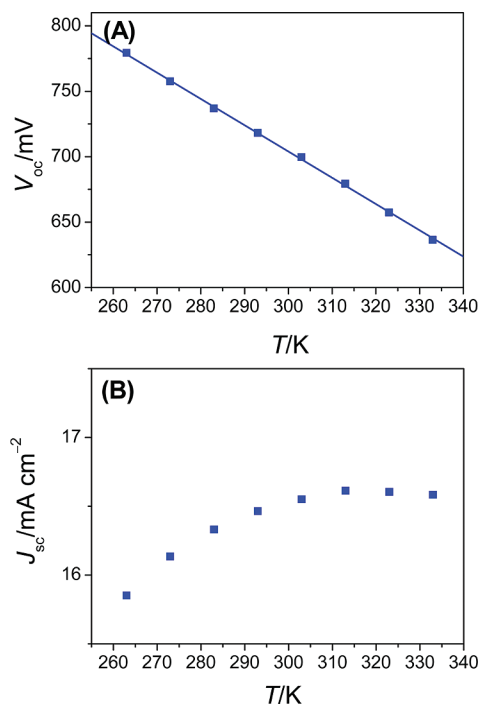**FIGURE 7. Error bar of efficiencies of the device A based on the LXJ-1 dye at various temperatures.**

FIGURE 8. Plots of temperature-dependent (A) open-circuit photovoltage and (B) short-circuit photocurrent for device A based on the LXJ-1 dye.
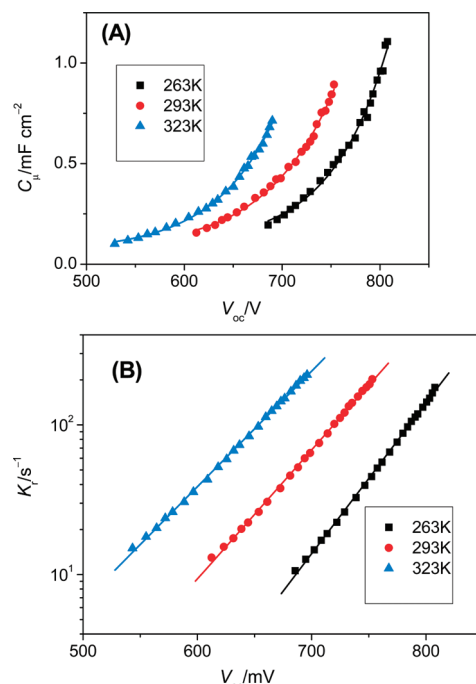

FIGURE 9. Plots of (A) chemical capacitance and (B) charge recombination rate constant versus open-circuit photovoltage for the device A made from LXJ-1 under various temperatures.

is 7.69 %. In addition, it is noted that dark currents for the DSC show a progressive enhancement along with the increase of temperature. This has been previously explained by Dittrich et al. (13) in terms of the notion of temperature-dependent recombination barrier height. As presented in Figure 8A, the open-circuit photovoltage decreases linearly along with temperature, from 797 mV at −20 °C to 636 mV at 60 °C, consistent with previous publications (14).

To clarify the change of the photovoltage-temperature, we resorted to the transient photoelectrical decay technique to measure the chemical capacitance(C_μ) and the charge recombination of device A at different temperatures. As presented in Figure 9A, the chemical capacitance(C_μ) of the cell increases along with the change in temperature at a given open-circuit photovoltage. We can derive from the chemical capacitance measurements that the density of surface states increases along with increasing temperature. We can calculate equilibrium potential of the electrolyte A at 50 °C which has a 5.39 mV negative shift with respect to

that at −10 °C. Apparently, higher C_μ at a higher temperature is related to more surface states in deep level contributing to the enlarged reverse saturation current, which has a significant effect on open-circuit photovoltage. This may explain the V_{oc} trend observed for different temperatures, because the V_{oc} decreases logarithmically with an increase in the reverse saturation current. And that a fast charge recombination with increasing the temperature will also be expounded, as shown in Figure 9B. We believe that all mentioned above could be mainly ascribed to enhanced diffusion coefficient of triiodide and electron trapped in the titania film at higher temperature.

The increase in J_{sc} along with the increase in temperature is shown in Figure 8B. We deduce that this current enhancement is related to a better charge collection. To scrutinize the effects of different temperatures on the electron collection in the mesoporous titania film, we further employed the dark electrical impendance measurments of the device A. As depicted in 10(A), the chemical diffusion coefficient of electron (D_n) is improved with the increase of temperature. However, with the increase of temperature electron lifetime (τ_n) is shortened rapidly as shown in Figure 10C. Furthermore, we have found from Figure 10B that the electron diffusion length (L_n) becomes short along with the increase of temperature, although it may be still enough for quantitative electron collection in the temperature range discussed here. Thereby, we suspect that the current enhancement is caused by an improved charge generation yield at a high temperature, which needs to be clarified in our further pump−probe measurements. Also, we found that the stable power conversion efficiencies at different
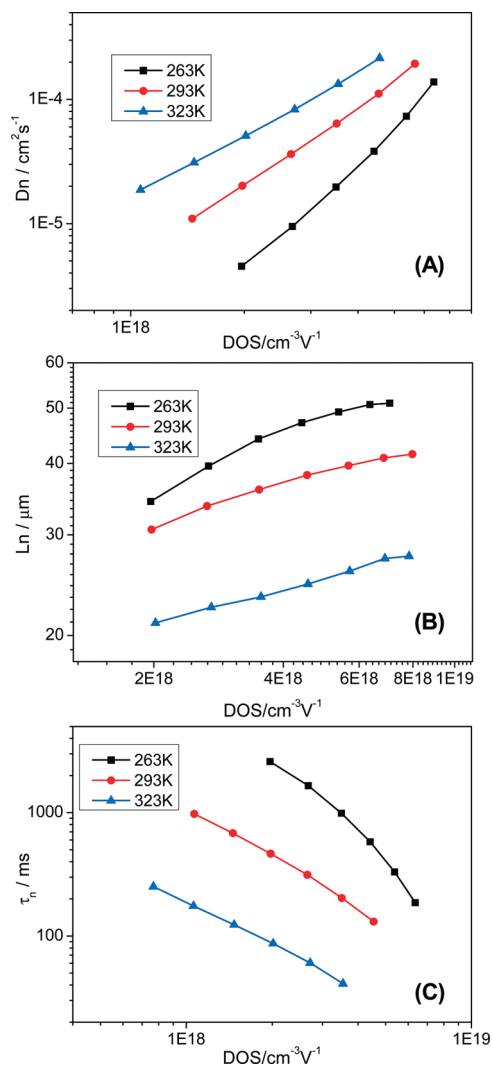
FIGURE 10. Plots of (A) electron diffusion coefficient, (B) electron diffusion length, and (C) electron lifetime versus DOS for the device A made from LXJ-1 under various temperatures.

FIGURE 11. Detailed photovoltaic parameters of the device C based on the LXJ-1 dye measured under an irradiance of 100 mW cm^{-2} AM1.5G sunlight during successive full sunlight soaking at 60 °C. Film thickness: 10 + 5. The ionic liquid electrolyte composition is DMII/EMII/EMITCB/I$_2$/NBB/GNCS (molar ratio: 12/12/16/1.67/3.33/0.67).

temperatures are due to a trade-off of the enhanced J_{sc} and the decreased V_{oc}.

For the cell of new dye, passing a long-term stability test is very critical to assess its potential for large scale application. Hence, we submitted our device C using the **LXJ-1** sensitizer along with a solvent-free ionic liquid electrolyte and covered it with a UV absorbing polymer film to the 1000 h accelerated testing at 60 °C in a solar simulator with a light intensity of 100 mW cm^{-2}. The cell shows good stability, keeping 96 % of its initial efficiency after 1000 h aging. The initial photovoltaic parameters (J_{sc}, V_{oc}, FF, and η) presented in Figure 11 are 11.27 mA cm^{-2}, 646.5 mV, 0.76, and 5.5 %, respectively.

4. CONCLUSIONS

In conclusion, we have synthesized a novel high molar extinction coefficient ruthenium sensitizer exhibiting an 8.8 % power conversion efficiency for an acetonitrile-based electrolyte in the AM 1.5G conditions. We further investigate temperature-dependent device physics and stability at 60 °C in a solar simulator with a light intensity
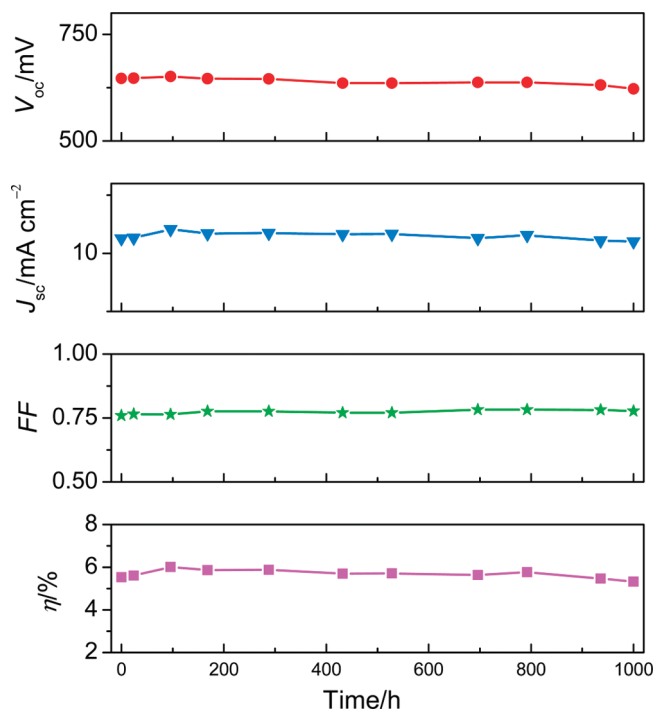
of 100 mW cm^{-2}. The enhanced J_{sc} due to better light harvesting is partially compromised with the loss in V_{oc} along with the increase of temperature. The overall power conversion efficiencies are stable not only at different temperatures but also at a long-term light. Therefore, we conclude that it is feasible and practicable that the new dye-sensitized solar cell will be produced on a large scale and applied outdoor at various temperatures.

REFERENCES AND NOTES

(1) O'Regan, B.; Grätzel, M. *Nature* **1991**, *353*, 737.
(2) Hagfeldt, A.; Grätzel, M. *Acc. Chem. Res.* **2000**, *33*, 269.
(3) Grätzel, M. *Nature* **2001**, *414*, 338.
(4) (a) Ferrere, S.; Gregg, B. A. *J. Am. Chem. Soc.* **1998**, *120*, 843. (b) Sauvé, G.; Cass, M. E.; Doig, S. J.; Lauermann, I.; Pomykal, K.; Lewis, N. S. *J. Phys. Chem. B* **2000**, *104*, 3488. (c) Asbury, J. B.; Hao, E.; Wang, Y.; Lian, T. *J. Phys. Chem. B* **2000**, *104*, 11957. (d) Kubo, W.; Kitamura, T.; Hanabusa, K.; Wada, Y.; Yanagida, S. *Chem. Commun.* **2002**, 374. (e) Paulsson, H.; Hagfeldt, A.; Kloo, L. *J. Phys. Chem. B* **2003**, *107*, 13665. (f) Hara, K.; Kurashige, M.; Dan-oh, Y.; Kasada, C.; Shinpo, A.; Suga, S.; Sayama, K.; Arakawa, H. *New J. Chem.* **2003**, *27*, 783. (g) Horiuchi, T.; Miura, H.; Sumioka, K.; Uchida, S. *J. Am. Chem. Soc.* **2004**, *126*, 12218. (h) Geary, E. A. M.; Yellowlees, L. J.; Jack, L. A.; Oswald, L. D. H.; Parsons, S.; Hirata, N.; Durrant, J. R.; Robertson, N. *Inorg. Chem.* **2005**, *44*, 242. (i) Kato, T.; Okazaki, A.; Hayase, S. *Chem. Commun.* **2005**, 363. (j) Martinson, A. B. F.; Elam, J. W.; Hupp, J. T.; Pellin, M. J. *Nano Lett.* **2007**, *7*, 2183. (k) Altobello, S.; Argazzi, R.; Caramori, S.; Contado, C.; Da Fré, S.; Rubino, P.; Choné, C.; Larramona, G.; Bignozzi, C. A. *J. Am. Chem. Soc.* **2005**, *127*, 15342. (l) Shi, D.; Pootrakulchote, N.; Li, R.; Guo, J.; Wang, Y.; Zakeeruddin, S. M.; Grätzel, M.; Wang, P. *J. Phys. Chem. C* **2008**, *112*, 17046. (m) Bai, Y.; Cao, Y.; Zhang, J.; Wang, M.; Li, R.; Wang, P.; Zakeeruddin, S. M.; Grätzel, M. *Nat. Mater.* **2008**, *7*, 626. (n) Yen, Y.-S.; Hsu, Y.-C.; Lin, J. T.; Chang, C.-W.; Hsu, C.-P.; Yin, D.-J. *J. Phys. Chem. C* **2008**, *112*, 12557. (o) O'Regan, B. C.; López-Duarte, I.; Martinez-Diaz, M. V.; Forneli, A.; Albero, J.; Morandeira,

A.; Palomares, E.; Torres, T.; Durrant, J. R. *J. Am. Chem. Soc.* **2008**, *130*, 2906. (p) Larisa, A. O.; Zaban, A. *J. Phys. Chem. C* **2008**, *112*, 2779. (q) Mihi, A.; Calvo, M. E.; Anta, J. A.; Míguez, H. *J. Phys. Chem. C* **2008**, *112*, 13. (r) Staniszewski, A.; Heuer, W. B.; Meyer, G. J. *Inorg. Chem.* **2008**, *47*, 7062.

(5) Cao, Y.; Bai, Y.; Yu, Q.; Cheng, Y.; Liu, S.; Shi, D.; Gao, F.; Wang, P. *J.Phys.Chem.C* **2009**, *113*, 6290.

(6) Cao, Y.; Zhang, J.; Bai, Y.; Li, R.; Zakeeruddin, S. M.; Grätzal, M.; Wang, P. *J.Phys.Chem.C* **2008**, *112*, 13775.

(7) (a) Maerker, G.; Case, F. H. *J. Am. Chem. Soc.* **1958**, *80*, 2745. (b) Wenkert, D.; Woodward, R. B. *J. Org. Chem.* **1983**, *48*, 283.

(8) Pilarski, B. *Liebigs Ann. Chem.* **1983**, 1078.

(9) Wang, P.; Zakeeruddin, S. M.; Comte, P.; Charvet, R.; Humphry-Baker, R.; Grätzel, M. *J. Phys. Chem. B* **2003**, *107*, 14336.

(10) (a) Chen, C.-Y.; Wu, S.-J.; Wu, C.-G.; Chen, J.-G.; Ho, K.-C. *Angew. Chem., Int. Ed.* **2006**, *45*, 5822. (b) Jiang, K.-J.; Masaki, N.; Xia, J.-B.; Noda, S.; Yanagida, S. *Chem. Commun.* **2006**, 2460. (c) Karthikeyan, C. S.; Wietasch, H.; Thelakkat, M. *Adv. Mater.* **2007**, *19*, 1091. (d) Chen, C.-Y.; Wu, S.-J.; Li, J.-Y.; Wu, C.-G.; Chen, J.-G.; Ho, K.-C. *Adv. Mater.* **2007**, *19*, 3888. (e) Chen, C.-Y.; Chen, J.-G.; Wu, S.-J.; Li, J.-Y.; Wu, C.-G.; Ho, K.-C. *Angew. Chem., Int. Ed.* **2008**, *47*, 7342. (f) Lee, C.; Yum, J.-H.; Choi, H.; Kang, S. O.; Ko, J.; Humphry-Baker, R.; Grätzel, M.; Nazeeruddin, M. K. *Inorg. Chem.* **2008**, *47*, 2267. (g) Mater, F.; Ghaddar, T. H.; Walley, K.; DosSanto, T.; Durrant, J. R.; O'Regan, B. *J. Mater. Chem.* **2008**, *18*, 4246.

(11) (a) Hagfeldf, A.; Grätzel, M. *Chem. Rev.* **1995**, *95*, 49. (b) Grätzel, M. *Nature* **2001**, *414*, 338.

(12) Zhang, G.; Bai, Y.; Li, R.; Shi, D.; Wenger, S.; Zakeeruddin, S. M.; Grätzel, M.; Wang, P. *Energy Environ. Sci.* **2009**, *2*, 92.

(13) Dittrich, T.; Beer, P.; Koch, F.; Weidmann, J.; Lauermann, I. *Appl. Phys. Lett.* **1998**, *73*, 1901.

(14) (a) Kron, G.; Egerter, T.; Werner, J. H.; Rau, U. *J. Phys. Chem. B* **2003**, *107*, 3556. (b) Snaith, H. J.; Zakeeruddin, S. M.; Schmidt Mende, L.; Klein, C.; Grätzel, M. *Angew. Chem., Int. Ed.* **2005**, *44*, 6413.

AM100285Z